Wound healing monitoring using near infrared fluorescent fibrinogen

Chia-Pin Pan,[1] Yihui Shi,[2] Khalid Amin,[3] Charles S. Greenberg,[4] Zishan Haroon,[5] and Gregory W. Faris[1,*]

[1]*Physical Sciences Division, SRI International, 333 Ravenswood Avenue, Menlo Park, CA. 94025, USA*
[2]*Biosciences Division, SRI International, 333 Ravenswood Avenue, Menlo Park, CA. 94025, USA*
[3]*Dept of Pathology and Laboratory Medicine, University of Kansas, 3901 Rainbow Blvd, Kansas City, KS 66160, USA*
[4]*Medical University of South Carolina, 96 Jonathan Lucas Street, Charleston, SC 29424, USA*
[5]*Carolina Institute for Nanomedicine, University of North Carolina, 1079 GMB, CB#7295, Chapel Hill, NC 27599, USA*
**gregory.faris@sri.com*

Abstract: We demonstrate a method for imaging the wound healing process with near infrared fluorescent fibrinogen. Wound healing studies were performed on a rat punch biopsy model. Fibrinogen was conjugated with a near infrared fluorescent dye and injected into the tail vein. Fibrinogen is a useful protein for tracking wound healing because it is involved in fibrin clot formation and formation of new provisional matrix through transglutaminase's crosslinking activity. Strong fluorescence specific to the wound was observed and persisted for several days, indicating that the fibrinogen is converted to crosslinked fibrin. Administration of contrast agent simultaneously with wound creation led to primary labeling of the fibrin clot, indicating that the wound was in its early phase of healing. Administration on the following day showed labeling on the wound periphery, indicating location of formation of a new provisional matrix. This method may prove to be useful as a diagnostic for basic studies of the wound healing process, in drug development, or in clinical assessment of chronic wounds.

OCIS codes: (170.2655) Functional monitoring and imaging; (170.6935) Tissue characterization; (170.4580) Optical diagnostics for medicine; (170.3880) Medical and biological imaging; (170.1610) Clinical applications.

References and links

1. L. Khaodhiar, T. Dinh, K. T. Schomacker, S. V. Panasyuk, J. E. Freeman, R. Lew, T. Vo, A. A. Panasyuk, C. Lima, J. M. Giurini, T. E. Lyons, and A. Veves, "The use of medical hyperspectral technology to evaluate microcirculatory changes in diabetic foot ulcers and to predict clinical outcomes," Diabetes Care **30**(4), 903–910 (2007).
2. A. J. Singer, and R. A. F. Clark, "Mechanisms of disease - Cutaneous wound healing," N. Engl. J. Med. **341**(10), 738–746 (1999).
3. R. Gillitzer, and M. Goebeler, "Chemokines in cutaneous wound healing," J. Leukoc. Biol. **69**(4), 513–521 (2001).
4. T. Kisseleva, and D. A. Brenner, "Mechanisms of fibrogenesis," Exp. Biol. Med. (Maywood) **233**(2), 109–122 (2008).
5. D. Telci, and M. Griffin, "Tissue transglutaminase (TG2)--a wound response enzyme," Front. Biosci. **11**(1), 867–882 (2006).
6. E. A. Verderio, T. S. Johnson, and M. Griffin, "Transglutaminases in wound healing and inflammation," Prog. Exp. Tumor Res. **38**, 89–114 (2005).
7. M. Griffin, R. Casadio, and C. M. Bergamini, "Transglutaminases: nature's biological glues," Biochem. J. **368**(2), 377–396 (2002).
8. C. S. Greenberg, P. J. Birckbichler, and R. H. Rice, "Transglutaminases: multifunctional cross-linking enzymes that stabilize tissues," FASEB J. **5**(15), 3071–3077 (1991).

#130226 - $15.00 USD Received 16 Jun 2010; revised 19 Jul 2010; accepted 19 Jul 2010; published 27 Jul 2010

9. S. Kojima, K. Nara, and D. B. Rifkin, "Requirement for transglutaminase in the activation of latent transforming growth factor-beta in bovine endothelial cells," J. Cell Biol. **121**(2), 439–448 (1993).
10. M. Siegel, P. Strnad, R. Watts, K. Choi, B. Jabri, G. Adler, B. Omary, and C. Khosla, "Extracellular transglutaminase 2 is catalytically inactive, but is transiently activated upon tissue injury in the small intestine," Gastroenterology **134**(4), A151 (2008).
11. E. A. Zemskov, A. Janiak, J. Hang, A. Waghray, and A. M. Belkin, "The role of tissue transglutaminase in cell-matrix interactions," Front. Biosci. **11**(1), 1057–1076 (2006).
12. C. S. Greenberg, K. E. Achyuthan, M. J. Borowitz, and M. A. Shuman, "The transglutaminase in vascular cells and tissues could provide an alternate pathway for fibrin stabilization," Blood **70**(3), 702–709 (1987).
13. D. C. Sane, T. L. Moser, A. M. M. Pippen, C. J. Parker, K. E. Achyuthan, and C. S. Greenberg, "Vitronectin is a substrate for transglutaminases," Biochem. Biophys. Res. Commun. **157**(1), 115–120 (1988).
14. D. H. Keast, C. K. Bowering, A. W. Evans, G. L. Mackean, C. Burrows, and L. D'Souza, "MEASURE: A proposed assessment framework for developing best practice recommendations for wound assessment," Wound Repair Regen. **12**(3 Suppl), s1–s17 (2004).
15. R. Salcido, "The future of wound measurement," Adv. Skin Wound Care **13**(2), 54, 56 (2000).
16. J. W. Griffin, E. A. Tolley, R. E. Tooms, R. A. Reyes, and J. K. Clifft, "A comparison of photographic and transparency-based methods for measuring wound surface area," Phys. Ther. **73**(2), 117–122 (1993).
17. D. J. Leaper, "Angiography as an index of healing in experimental laparotomy wounds and colonic anastomoses," Ann. R. Coll. Surg. Engl. **65**(1), 20–23 (1983).
18. M. J. Cobb, Y. C. Chen, R. A. Underwood, M. L. Usui, J. Olerud, and X. D. Li, "Noninvasive assessment of cutaneous wound healing using ultrahigh-resolution optical coherence tomography," J. Biomed. Opt. **11**(6), 064002 (2006).
19. T. Gambichler, G. Moussa, M. Sand, D. Sand, P. Altmeyer, and K. Hoffmann, "Applications of optical coherence tomography in dermatology," J. Dermatol. Sci. **40**(2), 85–94 (2005).
20. A. T. Yeh, B. S. Kao, W. G. Jung, Z. P. Chen, J. S. Nelson, and B. J. Tromberg, "Imaging wound healing using optical coherence tomography and multiphoton microscopy in an in vitro skin-equivalent tissue model," J. Biomed. Opt. **9**(2), 248–253 (2004).
21. M. Dyson, S. Moodley, L. Verjee, W. Verling, J. Weinman, and P. Wilson, "Wound healing assessment using 20 MHz ultrasound and photography," Skin Res. Technol. **9**(2), 116–121 (2003).
22. H. F. Zhang, K. Maslov, G. Stoica, and L. V. Wang, "Imaging acute thermal burns by photoacoustic microscopy," J. Biomed. Opt. **11**(5), 054033 (2006).
23. G. Mazooz, T. Mehlman, T. S. Lai, C. S. Greenberg, M. W. Dewhirst, and M. Neeman, "Development of magnetic resonance imaging contrast material for in vivo mapping of tissue transglutaminase activity," Cancer Res. **65**(4), 1369–1375 (2005).
24. F. A. Jaffer, D. E. Sosnovik, M. Nahrendorf, and R. Weissleder, "Molecular imaging of myocardial infarction," J. Mol. Cell. Cardiol. **41**(6), 921–933 (2006).
25. F. A. Jaffer, C. H. Tung, J. J. Wykrzykowska, N. H. Ho, A. K. Houng, G. L. Reed, and R. Weissleder, "Molecular imaging of factor XIIIa activity in thrombosis using a novel, near-infrared fluorescent contrast agent that covalently links to thrombi," Circulation **110**(2), 170–176 (2004).
26. J. M. Hettasch, N. Bandarenko, J. L. Burchette, T. S. Lai, J. R. Marks, Z. A. Haroon, K. Peters, M. W. Dewhirst, J. D. Iglehart, and C. S. Greenberg, "Tissue transglutaminase expression in human breast cancer," Lab. Invest. **75**(5), 637–645 (1996).
27. Z. A. Haroon, T. S. Lai, J. M. Hettasch, R. A. Lindberg, M. W. Dewhirst, and C. S. Greenberg, "Tissue transglutaminase is expressed as a host response to tumor invasion and inhibits tumor growth," Lab. Invest. **79**(12), 1679–1686 (1999).
28. J. M. Kollman, L. Pandi, M. R. Sawaya, M. Riley, and R. F. Doolittle, "Crystal structure of human fibrinogen," Biochemistry **48**(18), 3877–3886 (2009).
29. Z. A. Haroon, J. M. Hettasch, T. S. Lai, M. W. Dewhirst, and C. S. Greenberg, "Tissue transglutaminase is expressed, active, and directly involved in rat dermal wound healing and angiogenesis," FASEB J. **13**(13), 1787–1795 (1999).
30. S. A. Yuan, C. A. Roney, J. Wierwille, C. W. Chen, B. Y. Xu, G. Griffiths, J. Jiang, H. Z. Ma, A. Cable, R. M. Summers, and Y. Chen, "Co-registered optical coherence tomography and fluorescence molecular imaging for simultaneous morphological and molecular imaging," Phys. Med. Biol. **55**(1), 191–206 (2010).
31. H. F. Zhang, K. Maslov, G. Stoica, and L. V. Wang, "Functional photoacoustic microscopy for high-resolution and noninvasive in vivo imaging," Nat. Biotechnol. **24**(7), 848–851 (2006).
32. D. P. Pan, M. Pramanik, A. Senpan, X. M. Yang, K. H. Song, M. J. Scott, H. Y. Zhang, P. J. Gaffney, S. A. Wickline, L. V. Wang, and G. M. Lanza, "Molecular photoacoustic tomography with colloidal nanobeacons," Angew. Chem. Int. Ed. Engl. **48**(23), 4170–4173 (2009).
33. L. V. Wang, "Prospects of photoacoustic tomography," Med. Phys. **35**(12), 5758–5767 (2008).
34. K. H. Song, E. W. Stein, J. A. Margenthaler, and L. V. Wang, "Noninvasive photoacoustic identification of sentinel lymph nodes containing methylene blue in vivo in a rat model," J. Biomed. Opt. **13**(5), 054033 (2008).
35. H. Thangarajah, D. Yao, E. I. Chang, Y. Shi, L. Jazayeri, I. N. Vial, R. D. Galiano, X. L. Du, R. Grogan, M. G. Galvez, M. Januszyk, M. Brownlee, and G. C. Gurtner, "The molecular basis for impaired hypoxia-induced VEGF expression in diabetic tissues," Proc. Natl. Acad. Sci. U.S.A. **106**(32), 13505–13510 (2009).
36. L. F. Brown, K. T. Yeo, B. Berse, T. K. Yeo, D. R. Senger, H. F. Dvorak, and L. van de Water, "Expression of vascular permeability factor (vascular endothelial growth factor) by epidermal keratinocytes during wound healing," J. Exp. Med. **176**(5), 1375–1379 (1992).

#130226 - $15.00 USD Received 16 Jun 2010; revised 19 Jul 2010; accepted 19 Jul 2010; published 27 Jul 2010

37. Y. Sugimura, M. Hosono, F. Wada, T. Yoshimura, M. Maki, and K. Hitomi, "Screening for the preferred substrate sequence of transglutaminase using a phage-displayed peptide library: identification of peptide substrates for TGASE 2 and Factor XIIIA," J. Biol. Chem. **281**(26), 17699–17706 (2006).

1. Introduction

Wound healing is a dynamic and complex process involving several synchronized events that lead to blood clotting, healing of the wound site, and finally wound closure. Improper wound healing can lead to infection and severe complications that can lead to life-threatening conditions [1]. The healing cascade can be roughly divided into three overlapping phases: inflammation, proliferation, and tissue remodeling [2,3]. Tissue injury causes the leakage of blood from ruptured blood vessels into the extravascular space and induces platelet aggregation. Activated platelets promote thrombin formation that leads to fibrin clot formation. The clot provides primary protection for the damaged tissue and also acts as a provisional extracellular matrix (ECM). The coagulation pathway and injured cells also release various signaling mediators and chemotactic factors to recruit inflammatory leukocytes to the injury sites and initiate the healing process [4]. Once the wound is stabilized, re-epithelialization and proliferation processes start to form granulation tissue, replacing the fibrin clot and vascularizing the newly-growing tissue. The ECM in this phase is constantly degraded and reproduced to allow and support cell migration and tissue repair. During the remodeling phase, granulation tissue continues to be replaced and is transformed into scar tissue to reach the final resolution stage.

Transglutaminases (TGs) are cross-linking enzymes that are involved in several phases of the healing process [5,6]. The primary function of the TGs is to cross-link its substrates (various proteins and peptides) by catalyzing the formation of ε-(γ-glutamyl) lysine bonds (isopeptide bonds) between amide groups of glutamine and the primary amine group of various amines [7]. The resulting cross-linking products have higher resistance to chemical and enzymatic degradation [8]. The cross-linking function of the TGs is crucial in the formation of the provisional ECM during the healing process. TGs also serve as signaling molecules during the tissue repair process [9–11]. Many wound healing-related proteins have been identified as TG substrates (TGSub), such as fibrinogen, fibronectin, collagen, fibrin, and vitronectin [12,13]. At least two types of TGs are involved in the downstream coagulation cascade: thrombin-activated factor XIIIa, also called as plasma TG, which cross-links the fibrin monomers to form the fibrin clot; and tissue TG (TG2), which is expressed by epithelial cells around the wound site and is actively involved in the process of re-epithelialization and granulation tissue formation [4]. Other transglutaminases that can play a role include keratinocyte transglutaminase and epidermal transglutaminase.

Due to the complexity and diversity of wound conditions, current clinical wound assessment is typically performed through visual observation with or without the assistance of digital photography [14–16]. Dimensional and other qualitative information such as wound color, appearance, and location are collected for evaluating the healing progress. In general, these methods are somewhat subjective and the results are hard to quantify. In some cases, a histological examination that provides direct visualization of tissue is performed to assess if proper wound healing is occurring. However, histological examination involves sampling of the wound site, which in many cases can be difficult or even disruptive to already fragile tissue. Several groups are developing *in vivo* imaging techniques to monitor the wound healing process using angiography [17], ultrasound, optical coherence tomography (OCT) [18–21] and photoacoustic microscopy [22]. These techniques provide reasonable structural resolution and most importantly give a chance to observe the newly formed tissue underneath the scab. However, the techniques mostly focus on the observation of re-epithelialization, re-vascularization, and reformation of dermal-epidermal junction, events that are mainly related to late phases of the healing process, and do not provide the capability to identify specific biochemical defects in the healing process that would yield critical information to provide specific therapeutic intervention. TG has been shown to have multifunctional roles in the healing process. Mapping TG activity in the wound site could be used to monitor the

#130226 - $15.00 USD Received 16 Jun 2010; revised 19 Jul 2010; accepted 19 Jul 2010; published 27 Jul 2010

progression of wound repair [23]. The diverse categories of TGSub also provide an opportunity to distinguish the different stages of wound healing. Optical imaging of the TGSub distribution has been used to monitor the thrombosis process and healing after myocardial infarction [24,25]. Since the transglutaminases are also associated with tumor boundaries [26,27], this approach is also of interest for cancer imaging. Here, we demonstrate the use of near infrared fluorescent dye-labeled fibrinogen (a transglutaminase substrate) as a contrast agent to monitor the progression of the wound healing in rat dermal tissues.

2. Materials and methods

Abbreviations used in this paper are listed in Table 1.

Table 1. Abbreviations

BSA	bovine serum albumin
DMSO	dimethyl sulfoxide
DTT	(2S,3S)-1,4-bis-sulfanylbutane-2,3-diol or dithiothreitol
ECM	extracellular matrix
EDTA	2,2',2",2"'-(ethane-1,2-diyldinitrilo)tetraacetic acid
hFg	human fibrinogen
MW	molecular weight
MWCO	molecular weight cut off
NIR	near infrared
OCT	optical coherence tomography
SDS-PAGE	sodium dodecyl sulfate polyacrylamide gel electrophoresis
TG	transglutaminase
TG2	tissue transglutaminase
TGSub	transglutaminase substrates
VEGF	Vascular endothelial growth factor

2.1 Materials

Human fibrinogen (hFg) and bovine serum albumin (BSA) were obtained from Calbiochem. Near infrared (NIR) dye, HiLtye Fluor^{TM} 750 SE, was purchased from AnaSpec, Inc. All other chemicals were the highest grade available and used without further purification.

2.2 Labeling Fibrinogen and BSA

NIR labels were prepared following the suggested protocol provided by the vendor (AnaSpec). In brief, 0.15–0.25 μmole of hFg or BSA were dissolved in 100 mM Na_2CO_3/$NaHCO_3$ pH 8.0 buffer. NIR dye (0.75–2.22 μmole) was first dissolved in 20 μL DMSO and added to the buffer. The solution was kept at room temperature for 90–120 min. The unlabeled dye was then removed by centrifugal filtration using a membrane with a molecular weight cut off (MWCO) of 30,000 (Millipore). The resulting labeled protein was reconstituted in normal saline at a concentration of 12 μM (dye). The concentrations of dye and protein were determined by their absorbance at 754 and 280 nm, respectively.

The ability of the labeled fibrinogen molecule to function as a TG substrate was tested by reacting with unlabeled hFg (viable TG substrate) in presence of guinea pig liver TG2 (N-Zyme BioTec GmbH). Labeled hFg (13μg) and 4 μg labeled BSA were reacted with 10 μg unlabeled hFg in 150 mM NaCl, 5 mM DTT, 10 mM $CaCl_2$, and 50 mM Tris buffer at pH 8.3. TG2 activity is calcium dependent and should produce covalent high molecular weight complexes that would not readily enter a SDS-PAGE gel. EDTA (10 mM) was used to inhibit TG2 activity as a negative control. BSA is not a TG substrate and should not form high molecular weight complexes.

2.3 Imaging apparatus

NIR animal images were taken using a home-built imaging box as shown in Fig. 1. The camera was placed at top upright position and the excitation light sources were installed off-axially and tilted to the center of view (tilt angle = 22.5°). Two high-power 735 nm LEDs (Epitex L735-66-60) were used as the excitation light source. LEDs were used because they

#130226 - $15.00 USD Received 16 Jun 2010; revised 19 Jul 2010; accepted 19 Jul 2010; published 27 Jul 2010

provide high power at low-cost and do not have problems with speckle. Band pass filters (Chroma HQ710/75x) were used to cut off excitation light above 750 nm. The distances between LEDs and sample were approximately 33 cm. An Apogee Alta-U6 monochrome CCD digital camera was used to acquire images. For fluorescence images, a Chroma HQ780LP filter and a Schott RG665 filter were used to eliminate scattered excitation light. For the "white light" images (i.e., elastically scattered light showing the illumination distribution on the animal), we used the same LED illumination and a neutral density filter (O.D. = 4) in front of the camera to avoid overexposure. A filter wheel (Optec IFW) was installed to exchange the filters. The system was controlled by LabVIEW®. Background (dark) images were acquired using opaque cardboard in one of the filter wheel positions.

To acquire the images of dissected tissue with higher resolution, a scanning imager (LI-COR Odyssey) was used with the spatial resolution set at 21 μm.

2.4 Imaging Protocol

Fisher female rats (F344, 160–180 g, and 8–10 weeks old) were used for the animal imaging experiments. The rats were anesthetized during shaving, wound creation, and imaging using isoflurane inhalation (induction with 3-4% isoflurane for 30 seconds and maintenance with 1-2% isoflurane, with oxygen as the balance gas). Four wounds were created in pairs on the upper dorsum using a sterile punch. The labels were administered through tail vein injection.

The image resolution was set at 16 bits with 1 × 1 binning. For the fluorescence and background images, the exposure times were set at one second; for the "white light" images, the exposure was 0.2 second. The images were processed by MATLAB® or ImageJ.

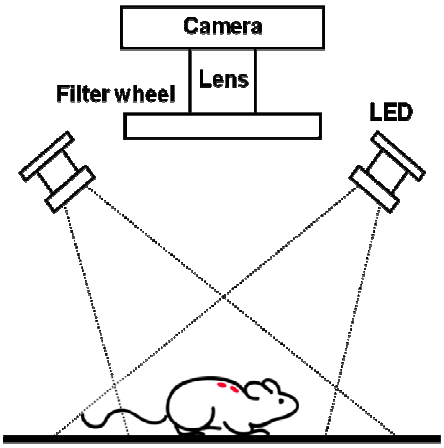

Fig. 1. Schematic of imaging system.

3. Results

3.1 NIR labels

The dye-to-protein (D/P) ratios of labels depend on the relative moles of NIR dye used in the conjugation reaction. The D/P ratio ranged from 1.2 to 4.4 for hFg labels and from 0.5 to 1.9 for BSA. Considering that only a trace amount of fibrinogen and albumin was injected into the rats, the difference of the D/P ratios between labels is not significant. However, to facilitate quantitative comparison of the fluorescence emitted from each rat from different labels, the total amounts of conjugated dye injected into the animal were kept constant. The images presented here used D/P ratios of 2.9 for hFg and 1.9 for BSA. The total amount of injected conjugated dye was 3 nmole.

To identify what chains of fibrinogen were labeled and whether labeling altered crosslinking of fibrinogen, the labeled proteins were cross-linked with unlabeled hFg. SDS-PAGE gels verified that the labeled proteins retained their TG2 activity as shown in Fig. 2.

#130226 - $15.00 USD Received 16 Jun 2010; revised 19 Jul 2010; accepted 19 Jul 2010; published 27 Jul 2010

The three bands that are shown in Coomassie blue staining (left panel) demonstrate that the α (63.5 kDa), β (56 kDa), and γ (47 kDa) chains of fibrinogen were comparably labeled [28]. The intensities of these three bands were either significantly reduced or disappeared when guinea pig liver TG2 was activated (lanes 4 and 8) and several high molecular weight bands developed, indicating that cross-linking products were formed and may not have entered the SDS-PAGE gel. The NIR image (right panel) shows that the hFg label (lanes 3–5) exhibits the same pattern as seen with the Coomassie blue staining, while the BSA label shows only limited influence from the presence of activated TG2. Both observations suggest that the TGSub and control labels were labeled and reacted with TG2 as expected.

3.2 Wound imaging

The LEDs were operated at an output of 550 mW (per LED). The net output after the excitation filter was 80 mW (per LED). The rat was positioned so that the wound area would receive the maximum light distribution. The average power density at wound area was 0.7 mW/cm^2. The inhomogeneity over the wound area was 3% and that across the whole rat body (not including the limbs and tail) was less than 22%. The HQ780LP filter has leakage up to 59% from 380 to 520 nm. Although the imaging box was built as light-tight as possible and the room light was dimmed during the experiments, a RG665 filter was also placed in front of camera as a precaution against the potential exposure to visible light. The wound images were analyzed without further normalization for light input but corrected by subtracting the background (dark) images acquired with the same exposure time. The image resolution was about 0.25 mm per pixel. To better monitor the overall performance and sensitivity of the imaging box, a small piece of paper with multiple coats from a purple marker was placed by the animal as an internal reference [the orange square at the right of the "NIR fluorescence" image in Fig. 3(a)]. The fluorescence intensity from this internal reference is recorded and calculated. The fluctuation for all images over the experimental period is less than 8%.

The labels were injected via the tail vein. In case of excess bleeding before the label administration, the blood could quickly form fibrin gel in absence of the label. The scab developed from label-free fibrin would block fluorescence. To avoid this complication, the wound creation only punched through the dermis layer and kept the underlying tissues intact. Figure 3 shows the NIR fluorescence images of the punch wounds. The labels were administered within one hour after wound creation for all images in this figure. Using the hFg label as the contrast agent [Fig. 3(b)], the images show that the fluorescence contrast is strong and concentrated at the wounds. The contrast difference between wounded and normal tissues is substantial. For the BSA label [Fig. 3(c)], the images show that the contrast is medium to strong and dispersed over the upper dorsum. While one can still identify the wounds, the contrast difference between wounded and normal tissues is moderate on the images of first 48 hours and much less significant for the rest. Time-lapse images acquired each day over the course of healing reveals that the strongest contrast of the hFg label is primarily associated with the scabs and can last over 3 days until the scabs fall off from the wounds, indicating that the hFg label is cross-linked into the fibrin by factor XIIIa or TG2. In contrast, the "Day 1" (24 hours after administration of the contrast agent) image for the BSA label shows that the contrast distribution is in dispersed pattern over the upper dorsum and not specifically associated with the wounds. The contrast is significantly reduced in the Day 2 images and thereafter. This dispersed pattern suggests that the BSA label is leaked out from the circulation and temporarily deposited around the wounded tissue. The enhanced permeability of blood vessels was a hallmark of an acute inflammation response, which also takes place in the early phase of the wound healing. The significant reduction of the BSA label contrast within the central zone of fibrin formation indicates that the BSA label is not preferentially immobilized at the wound site by blood coagulation due to its lack of reactivity with fibrin and TGs.

#130226 - $15.00 USD Received 16 Jun 2010; revised 19 Jul 2010; accepted 19 Jul 2010; published 27 Jul 2010

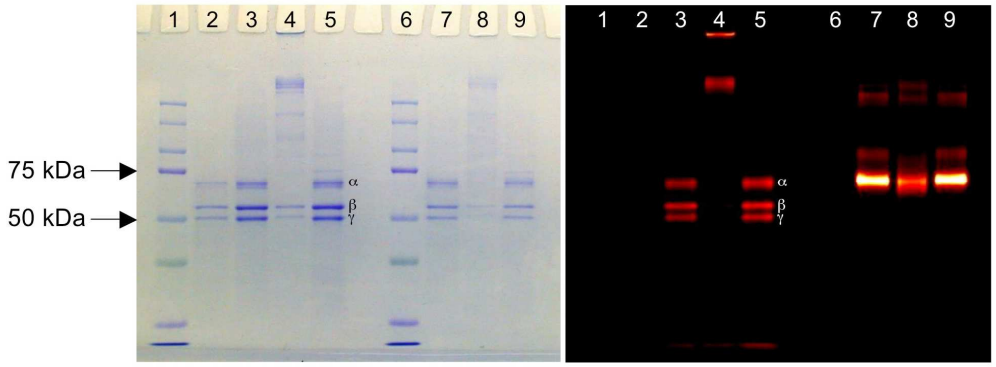

Fig. 2. SDS-PAGE gel images showing Coomassie blue staining (left panel) and NIR fluorescence (right panel) for the same gel. Lanes 1 and 6 are protein MW standards. Lane 2 is unlabeled hFg only. Three major bands (from top to bottom) represent α (63.5 kDa), β (56 kDa), and γ (47 kDa) chains, respectively. Lanes 3–5 and 7–9 are protein with NIR labels (3–5: hFG and 7–9: BSA) Lanes 3 and 7 have no TG2. Lanes 4 and 8 are incubated with TG2. Lanes 5 and 9 are incubated with both TG2 and EDTA. EDTA inhibits the cross-linking reaction of TG2.

Quantitative analysis of the same data set [Fig. 4(a), solid lines] shows similar trends to the direct observations of Fig. 3. Administration of the hFg label 24 hours after wound creation [dashed lines in Fig. 4(a)] produces fluorescence intensity decays that are quite similar to those with label administration on the same day as wound creation [solid lines in Fig. 4(a)]. This documents that fibrin formation and stabilization by TGs can continue after the fibrin clot appears to have formed an adequate barrier to blood loss. A recent study monitoring TG expression in a punch biopsy model in rats also shows a strong increase in TG expression between the day of the wound and the 24-72 hrs after the wound administration [29] The distribution of hFg label one day after wounding may be a combination of crosslinking and continued formation and degradation of fibrin at the site of tissue injury. For the BSA label, comparing the "Day 1" image for BSA label injection within one hour after wound creation [Fig. 3(c)] with the "Day 1" image for BSA label injection 24 hours after wound creation [Fig. 4(c)] shows that the later injection produces much less contrast from the tissue beneath the wounds, indicating that there is a reduced inflammation reaction around the wound sites after 24 hours.

3.3 Monitoring the progression of wound healing

The progression of wound healing strongly depends on the depth, size, position, and cause of the wound, as well as the physiological condition of the animal or individual. Considering the scope of this study, the dermal wound created by punch biopsy was adopted as the wound model to avoid excess bleeding, severe infection, and possible complications due to the wound creation in deep tissues. However, to examine the potential use of hFG label for tracking the progression of wound healing, hFG label was administrated at different time points after wound creation and the distribution patterns of the hFG label were carefully compared.

The early phase of the healing process involves hemostasis over the wound site, which provides protection for the damaged tissue and prevents further injury. Plasma TG (Factor XIIIa) plays a significant role in this step by cross-linking TG substrates to form the initial ECM. In the presence of dye-labeled TG substrate at this stage, the label should deposit over the wound sites as part of fibrin clot. The "Day 2" image collected from administering the hFg label within one hour after wound creation shows an even brightness at the center and edge of wound [Fig. 5(a)], consistent with this pattern. After the acute inflammatory response, the healing process starts to advance to the proliferation phase. In this phase, epithelial cells start to express TG2 to initialize the re-epithelialization process. The "Day 2" image from the hFg label administered 24 hours after wound creation [Fig. 5(b)] shows a stronger contrast at the

#130226 - $15.00 USD Received 16 Jun 2010; revised 19 Jul 2010; accepted 19 Jul 2010; published 27 Jul 2010

wound boundary but not at the center, indicating that higher TG activity is found in the surrounding epithelial tissue.

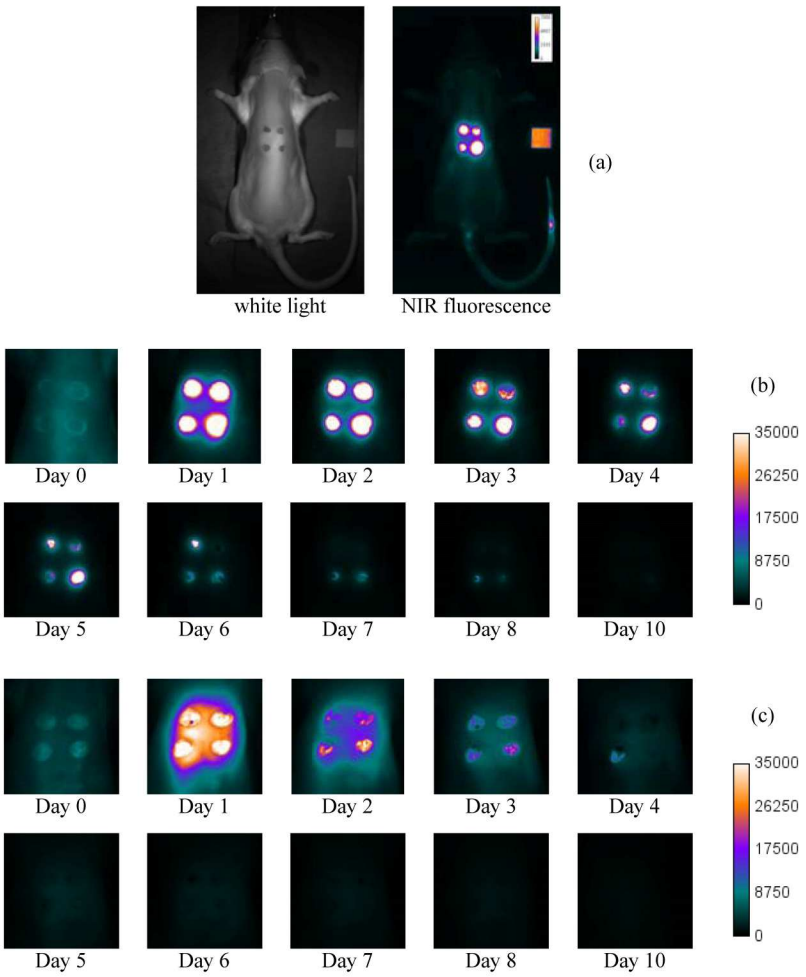

Fig. 3. Wound images. (a) Typical "white light" and NIR fluorescence images. The images in (b) and (c) are the expanded time-lapse images of wound sites, showing hFg label and BSA label respectively. The Day 0 image was taken within 5 min of contrast injection. Day 1 was taken 24 hrs after injection, Day 2, 48 hours after injection, and so forth.

Figure 5(c) shows an image acquired with the Odyssey® of a 10 μm-thick tissue section harvested from the rat administered with the hFg label 24 hours after wound creation at the time point of "Day 2" [48 hours after the injection, the same conditions as Fig. 5(b)]. The green is from the 800 nm channel and the red is from the 700 nm channel, representing NIR fluorescence and auto-fluorescence, respectively. The hFg label (green) is deposited around the wound, indicating high TG activity at that region which is consistent with the observation using the macro imaging system [Fig. 5(b)]. The width of hFg labeled ring is estimated about 1 mm.

#130226 - $15.00 USD Received 16 Jun 2010; revised 19 Jul 2010; accepted 19 Jul 2010; published 27 Jul 2010

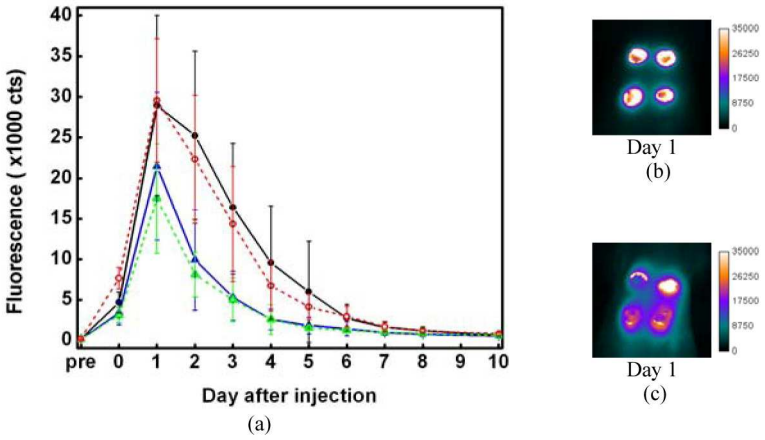

(a) (b) (c)

Fig. 4. (a) Plot of fluorescence intensity vs. time. The intensities were integrated from the wound individually. 8-12 wounds were inspected. The error bars describe the standard deviations of the intensity distribution. Solid lines represent the fluorescence changes for administration of the labels 1 hr after wound creation. Dashed lines are for administration of the labels 24 hrs after wound creation. Black and red: hFg. Blue and green: BSA. (b) and (c) are "Day 1" image (24 hrs after label administration) of the wound, for which the labels were injected into rat 24 hrs after wound creation. (b) is for hFg label. (c) is for BSA label.

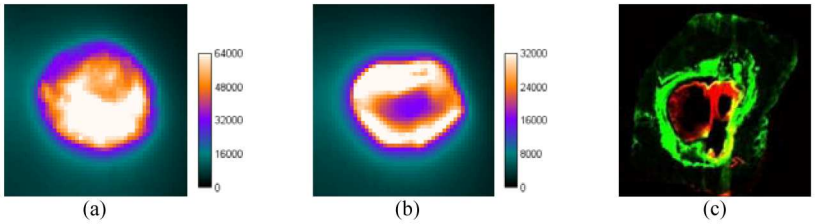

(a) (b) (c)

Fig. 5. "Day 2" images of wounds taken from giving hFg labels within 1hr (a) and 24 hrs (b) after wounding. (c) Tissue section of wound site.

4. Discussion and Conclusions

The wound healing process involves numerous signaling molecules, factors and mechanisms, which are also associated with a wide range of disease states. An unhealed wound or wound with prolonged healing time often indicates that there are serious health concerns for the patient. It is well known that wound healing is impaired in a diabetic foot ulcer. Approximately 90% of all low-extremity amputations happen in diabetic patients whose leg wounds failed to heal. Bedsores, or pressure ulcers, are developed in patients who are immobile or confined to beds because of disease or trauma. The prolonged healing time of these ulcers may progress to severe systemic infections. Under these situations and others, precise monitoring of the wound healing process would give valuable information for effective treatment. There are currently no methods that can provide a dynamic image of the process of fibrin formation and stabilization at sites of wound healing.

Molecular imaging uses the contrast agent to target specifically a particular biological pathway, and gives an image that contains not only the structural information but also the functional status of the process. In this study we perform conventional fluorescence imaging, which is both simple and sensitive. However, there are other imaging modes that provide additional information such as depth resolution or structural information at the expense of

#130226 - $15.00 USD Received 16 Jun 2010; revised 19 Jul 2010; accepted 19 Jul 2010; published 27 Jul 2010

greater complexity of the imaging system. For example, the recent development of fluorescence-guided optical coherence tomography uses fluorescence molecular imaging as the guide to obtain high resolution OCT images [30]. Another example is functional photoacoustic imaging [31–34], which benefits from molecular functionality and resolution of the image depth. Two photon microscopy provides optical sectioning through the nonlinear response with focal intensity, and can so also provide depth resolution. Here, we demonstrated use of NIR fluorescent hFg labels as contrast agents to monitor the wound healing process. We found that the fibrin formation and stabilization process is a dynamic event that continues for up to 24 hours after blood loss has stopped. Furthermore, the tissue surrounding the primary hemostatic fibrin clot remains permeable and deposits additional fibrin, it is currently unknown whether a wound that fails to heal continues to produce local fibrin and/or has a defect in depositing fibrin in the surrounding tissue to promote wound healing. Vascular endothelial growth factor (VEGF), a molecule that promotes cell migration and vascular permeability early during would healing, is reported to be defective in diabetic wounds [35]. VEGF expression could be used as a molecular marker to assess the permeability changes during wound healing [36]. The use of this technique could further define whether wounds in diabetes form stable clots or have fibrin clots that fail to deposit fibrin in the adjacent tissue.

For injection on the day of the wound, the labeled fibrinogen deposits in the wound because thrombin generated at the site of blood clotting converts the soluble fibrinogen to a fibrin gel. The fibrin becomes stable by the crosslinking action of factor XIIIa. When fibrinogen is injected after the clot forms it is very likely that it gets cross-linked into the matrix by the enzymatic action of transglutaminases that are in the tissue, as supported by the patterns of hFg labeling [Figs. 5(b) and 5(c)] and previous studies using immunohistochemical staining [29]. Fibrin is a complex network of fibrin fibers that localizes where thrombin is generated and converts soluble fibrinogen to polymerizing fibrin molecules. Fibrin molecules polymerize end-to-end and side-by-side producing a highly concentrated network of fibrin molecules that would be highly fluorescent. Compared with the other enzymatic mechanisms of contrast formation, fibrin polymerization and a cross-linking mechanism that localizes and makes the molecule resistant to degradation would generate a stronger and more persistent contrast. The trade-off for this mechanism is the speed of contrast formation. The circulation time of TGSub labels may also be varied to optimize this imaging strategy. The longer the circulation time, the stronger the resulting contrast. However, if the circulation time of the TGSub label were too long, it would be less useful for monitoring fast-paced wound healing processes. As aforementioned, at different phases of wound healing process, different subtypes of TG are involved. It would be very beneficial to develop TGSub labels which selectively target at certain subtype of TGs. Hitomi *et al.* have developed two phage-displayed peptide libraries of TG substrates that show strong in vitro selectivity to factor XIIIa and TG2, respectively [37]. We are currently developing peptide-based TGSub labels with optimized circulation times and selectivity to different TG subtypes to address these opportunities.

Acknowledgement

This work was supported by the DOD Breast Cancer Research Program, Grant Number W81XWH-05-1-0386, and the National Cancer Institute, Grant Number 1R21 CA107285.

#130226 - $15.00 USD Received 16 Jun 2010; revised 19 Jul 2010; accepted 19 Jul 2010; published 27 Jul 2010